LAWRENCE
LIVERMORE
NATIONAL
LABORATORY

LLNL-CONF-420370

The effect of pulse duration on the growth rate of laser-induced damage sites at 351 nm on fused silica surfaces

R. A. Negres, M. A. Norton, Z. M. Liao, D. A. Cross, J. D. Bude, C. W. Carr

November 18, 2009

Boulder Damage Symposium
Boulder, CA, United States
September 20, 2009 through September 23, 2009

Disclaimer

The effect of pulse duration on the growth rate of laser-induced damage sites at 351 nm on fused silica surfaces

*R. A. Negres, M. A. Norton, Z. M. Liao, D. A. Cross, J. D. Bude and C. W. Carr
Lawrence Livermore National Laboratory
7000 East Avenue, Livermore, CA 94550, USA

ABSTRACT

Past work in the area of laser-induced damage growth has shown growth rates to be primarily dependent on the laser fluence and wavelength. More recent studies suggest that growth rate, similar to the damage initiation process, is affected by a number of additional parameters including pulse duration, pulse shape, site size, and internal structure. In this study, we focus on the effect of pulse duration on the growth rate of laser damage sites located on the exit surface of fused silica optics. Our results demonstrate, for the first time, a significant dependence of growth rate at 351 nm on pulse duration from 1 ns to 15 ns as $\tau^{0.3}$ for sites in the 50-100 μm size range.

Keywords: laser-induced damage, surface damage growth, fused silica

1. INTRODUCTION

Laser-induced growth of optical damage can potentially limit the fluence at which optical components may be used. Hence, numerous studies[1-8] have been dedicated to the growth problem, primarily on fused silica optics. The different experimental apparatus and techniques used by various research groups make interpretation and comparison of the results a nontrivial task. One fact that stands out is the complexity of the growth process due to the many laser, material and experimental parameters involved, such as wavelength[2,4-8], fluence[1-8], pulse duration and pulse shape[1-3,9-11], surface[1-3,12,13] (input/exit, coated and bare), site morphology[8,14-16], beam size[1,17,18], and growth environment (air/vacuum)[2].

Here we will restrict our discussion to surface damage growth under very specific experimental conditions: i) flooded fluence conditions using large aperture laser beams (leading to growth in the lateral dimensions of the site, as opposed to using small area beams typically employed in drilling operations associated with growth in the depth of the site[15,16]) and ii) bare surfaces of fused silica substrates in vacuum (for the reasons stated below in the experimental section). We note that previous studies under similar fluence conditions in air (~10 Torr) vs. vacuum and bare vs. coated surfaces[1-2] did not show significant differences in the growth behavior at 351 nm. This is in contrast to the distinct laser damage initiation characteristics at 351 nm of coated vs. uncoated silica surfaces in various environments[19,20].

Most of the past growth experiments[1-5] were conducted using single wavelength, ns pulses, at the first, second and third harmonics of 1053 nm (Nd:glass lasers), and indicated that damage growth with UV pulses exhibits the lowest fluence growth threshold at ~5 J/cm^2 in contrast to ~12 J/cm^2 at 527 nm and ~15 J/cm^2 and 1053 nm, respectively. These threshold values are generally valid for both exit and input surfaces, although the input surface appears to exhibit a somewhat higher threshold (by ~1 J/cm^2) than the exit surface under similar conditions[12]. In addition, the slope of the exponential growth coefficient vs. fluence is highest for 351nm. For the case when multiple wavelengths are present simultaneously, for example 1053 nm and 351 nm, the growth behavior has been described, to the first order, by the 351-nm growth coefficient evaluated at the total fluence, i.e. as if all of the laser energy was delivered at 351 nm[6-8].

Previous work at LLNL[1-2] aimed at elucidating the effects of pulse length on the exit surface growth rate at 351 nm in the 1-11 ns range suggested only a weak dependence as $\tau^{0.1}$. However, the data was primarily obtained at longer pulses (9 ns and 11 ns, near Gaussian shape) with fluences from 5 J/cm^2 up to 12 J/cm^2. In contrast, only a few damage sites were examined using shorter pulses (1 ns and 3ns) over a narrow range of fluences (4-6 J/cm^2). Similarly, other research

* negres2@llnl.gov; phone 1-925-423-1425; fax 1-925-422-5718

groups[3,7] have reported on the damage growth at 351 nm with pulse durations of ~3 ns with limited site statistics and their results appeared to support the weak or no pulse-length dependence to the growth rate.

The previous growth studies[2,8] have also briefly noted a dependence of growth on site morphology, including the size and the type of damage initiation, for example laser damage vs. mechanical indentation. Specifically, small sites (up to 100 μm in diameter) appear to grow much more aggressively than larger sites in the range of ~200-300 μm diameters. In addition, mechanical indents were observed to consistently grow ~ 20% faster than sites initiated with 351 nm laser pulses.

In this work, we will expand the knowledge base of single wavelength damage growth by investigating the effects of pulse duration on the growth of laser-induced damage sites on the exit surface of silica optics under 351-nm laser irradiation. Using pulses with flat-in-time (FIT) temporal profiles, we measure the growth parameters for sites with diameters in a narrow size range as a function of pulse duration from 1 ns to 15 ns. In addition, we employ a large aperture laser beam to simultaneously grow a large number of sites for better growth statistics.

2. EXPERIMENTAL TECHNIQUES

2.1 Sample preparation

The samples were 2-inch in diameter and 1-cm thick UV grade Corning 7980 glass windows obtained from multiple vendors and prepared to achieve high quality surfaces with high damage resistance by LLNL-developed etching and cleaning procedures. We then employed a table top Nd:YAG laser with near Gaussian temporal and spatial profiles to induce an array of 40 to 60 similar damage sites on the exit surface. Typically, damage sites of ~40-60 μm in diameter were initiated in a regular grid pattern on the sample's exit surface using a single pulse at 355-nm with ~30 J/cm^2 (within 15%), 7 ns at Full-Width-Half-Maximum (FWHM) and a beam diameter of ~450 μm (at FW1/e^{2}M). At some locations on the exit surface, the resulting damage pits were smaller than 40 μm as observed by the online microscope; therefore subsequent pulses (one or two) were used to grow the individual sites at a lower fluence of ~15 J/cm^2 to achieve damage sites of similar size. A dozen or so samples were prepared using the above procedure with the spacing of 3 mm or 4 mm within each row and between adjacent rows, resulting in a total of 58 or 38 sites within a 3-cm aperture, respectively. The 58-site arrangement is illustrated in Fig. 1(a). For either grid spacing, we found no measurable cross-talk between adjacent damage sites for growth diameters up to about 1 mm; closer packing of the sites is feasible if growth diameter is limited to ~500 μm. Figure 1(b) shows the typical distribution of sizes on a sample and Fig. 1(c) shows an example of typical single- and multi-pit small beam initiation morphologies. Alignment fiducials, placed near the edge of the aperture aid in the fluence registration. The fiducials were applied with a CO_2 laser technique that creates ~100 μm-diameter laser-evaporated pits that are damage resistant up to ~10-12 J/cm^2.

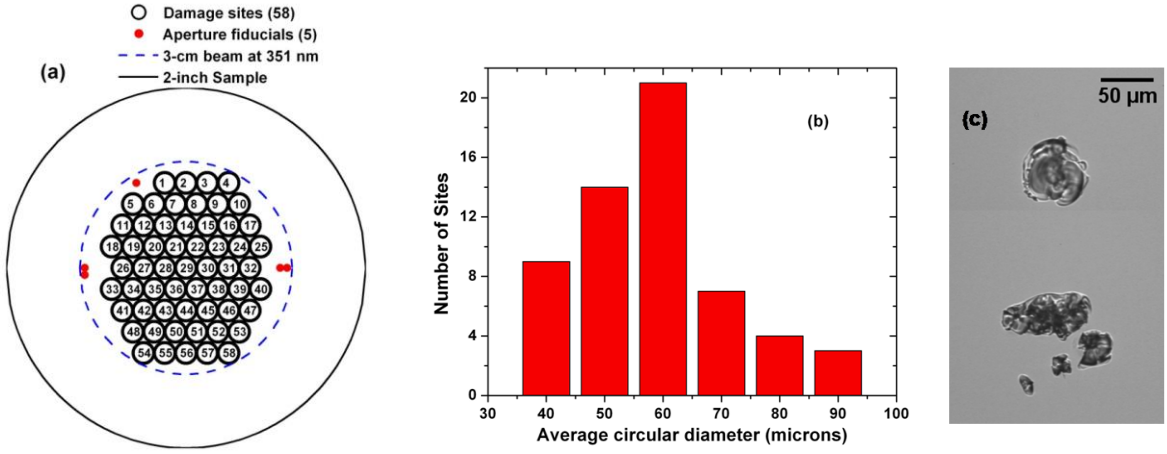

Figure 1 (color online). a) Sample layout with 58 laser-initiated damage sites in a regular grid (3-mm spacing) and 5 fiducials within the footprint of the 3-cm test beam. b) An example of size distribution for 58 damage sites as prepared with a small beam. c) Micrographs of typical single and multi-pit damage sites using back-light illumination.

2.2 Growth methodology

All experiments presented in this work were conducted at the Optical Sciences Laboratory (OSL) at LLNL. This facility hosts a large aperture, Nd:glass, 10-cm disk amplifier laser system with an adjustable pulse width and shape.[18] The OSL laser can fire a single, 50 J pulse at 351 nm with high quality beam profile at a repetition rate of one shot every 45 minutes. The growth experimental layout using the OSL laser is similar to that described by Norton et al. for the SLAB laser.[2] The sample is positioned in an image relay plane of the laser and is housed in a stainless steel vacuum chamber, which is in turn located in a class 100 clean room where samples up to 150 mm x 150 mm in size are handled during loading. The beam size at 351 nm on the part is nominally 30 mm in diameter. We take advantage of the large area beam provided by the OSL laser system to grow simultaneously a large number of sites making this a high throughput experiment despite the relatively low laser repetition rate. Laser beam diagnostics for the test beam on the part include measurements of the temporal pulse shape, energy and input & output beam near field fluence profiles. All test series were conducted in vacuum at room temperature.

The growth experiments were performed using the large-area beam at fixed fluence ranging from 5 J/cm^2 up to 12 J/cm^2 for 15 up to 30 shots with discrete pulse durations between 1 ns and 15 ns at 351 nm (i.e., 1, 2, 5, 10 and 15 ns, all FIT). Fresh samples with pre-initiated sites as discussed above were used for each fluence/pulse duration combination. The typical temporal profiles measured using 60-ps rise time photodiodes are shown in Fig. 2(a). The input and output beam near field fluence profiles acquired during a laser shot are illustrated in Fig. 2(b). These images are acquired by CCD cameras placed at image relay planes with respect to the sample's exit surface location. The input camera is calibrated for energy and magnification to record the fluence map on any given shot with a spatial resolution of about 88.3 microns/pixel. The near flat-top spatial beam profile has a typical contrast of 16-18% for the above growth fluences. The output camera records the beam profile after passing through the sample; hence the locations of the reference fiducials are also captured in this image as indicated by the red circles in Fig. 2(b). We note that the array of damage sites also becomes visible in the output image for laser shots later in the growth sequence, after the sites reach about ~100 μm in diameter. We use the locations of the fiducials relative to beam features present in both input and output images to accurately superimpose the site location map onto the input fluence image. We are then able to extract the local fluence in a ~1 mm patch at individual site locations during every laser shot. The local fluence/site registration can be performed within 200 μm (~ 2 image pixels). The measurement uncertainty in the laser pulse energy is about 5% thus the overall uncertainty in the local fluence at damage site locations is estimated to be not more than 10-15% given the spatial uniformity of the laser beam profile at 351 nm. The local fluence calibration methods used in this study were previously developed in an effort to improve the qualitative and quantitative measurements of laser-induced damage[21].

The growth in the lateral size of the damage sites simultaneously exposed to a single OSL laser pulse is measured off-line (outside the vacuum chamber) using a robotic microscope that records backlit images of all sites before and after each laser shot with ~1 μm resolution. Throughout this work, the effective circular diameter of individual pits as derived from image auto-thresholding will be used as the metric for the damage site size. The minimum shot-to-shot absolute change in diameter of a site, as detected with our microscope system, is about 2 μm. This instrument error is a combination of i) slight changes in the image lighting every time the sample is repositioned on the microscope translation stage for post-shot scanning and ii) subtle modifications in the damage site morphology, for example the onset of subsurface cracks, which are not consistently captured in the damage area as reported by our image thresholding software routine. For a narrow range of damage site sizes, we will estimate the noise floor associated with the single-shot growth coefficient based on the ~ 2 μm sizing error.

The 'multi-site parallel damage growth' technique described above can be summarized as follows:

- Step 1: preparation of a large number of similar damage sites in a regular pattern on the exit surface of a fused silica substrate using a small area laser beam
- Step 2: pre-shot measurement of individual site diameters using a robotic microscope
- Step 3: simultaneous exposure of all sites with a single laser pulse (large area beam) and recording of input and output near field beam profiles
- Step 4: post-shot measurement of individual site diameters using a robotic microscope, the same as step 2
- Steps 3 and 4 are repeated for all shots in the growth sequence for a given sample

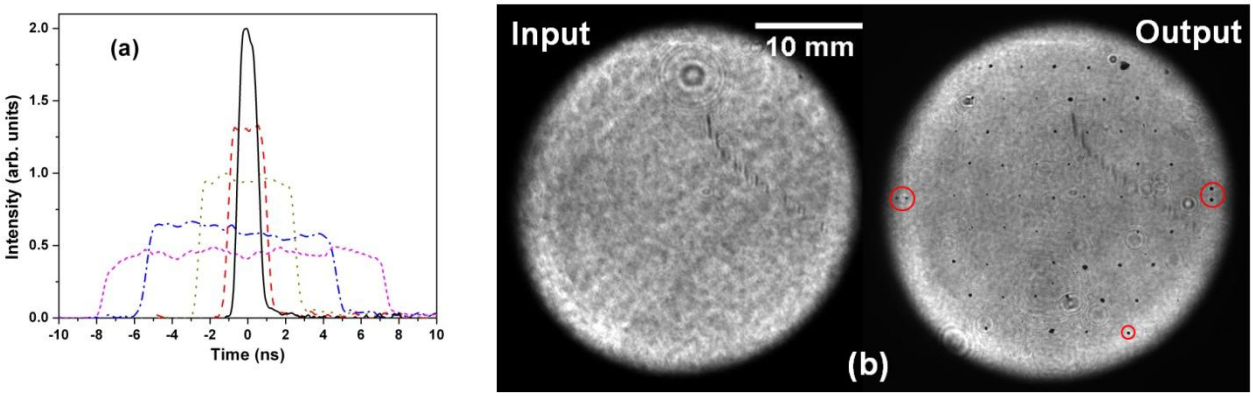

Figure 2 (color online). (a) Typical temporal profiles for 1, 2, 5, 10 and 15 ns duration pulses at 351 nm used in experiment. (b) Input and output near field fluence profiles of a typical laser shot. The ~100-μm CO_2 fiducials (indicated by red circles) are always visible in the output image allowing precise registration of the local fluence to an individual site on every laser shot.

3. ANALYSIS TECHNIQUES FOR SINGLE-SHOT GROWTH

Historically, the exit surface damage growth has been generally described by an exponential increase in diameter with the number of shots at fixed fluence, as follows:

$$d_N = d_0 \exp(\bar{\alpha} \cdot N), \tag{1}$$

where d_N represents the diameter of the site after N shots at fixed fluence and $\bar{\alpha}$ represents the average exponential growth coefficient. In practice, the growth coefficient (dimensionless) is found by plotting the measured site diameter during the growth sequence vs. shot number and fitting the data to an exponential curve. This procedure is repeated for many sites grown at different fluences to reveal that the average growth coefficient increases linearly with 351-nm fluence:

$$\bar{\alpha}(\phi) = 0.0392 \cdot (\phi - 5), \tag{2}$$

where the fluence ϕ is expressed in J/cm^2. Various research groups have confirmed the validity of Eq. (2) with small variations on the coefficients. However, Eq. (2) was derived primarily from growth data obtained with 10-12 ns, Gaussian pulses and for large sites starting at 100-200 μm and growing up to 1-2 mm in diameter[2]. Therefore, care must be taken when comparing growth results for different pulse durations and damage size ranges, in particular for sites smaller than 100 μm.

The data analysis outlined above is a multi-shot analysis approach in which the growth coefficient, $\bar{\alpha}$, is used to describe the average growth behavior of damage sites for multiple shots (N~30). This procedure can quickly become time consuming for parameter studies that require a large number of sites at discrete growth fluences to achieve good statistics. Therefore, we adopt a different analysis approach to study the effects of pulse duration on the growth parameters at 351 nm. Specifically, we define the single-shot growth coefficient, α, based on the expectation of perfect exponential growth between two consecutive shots, as follows from Eq. (1):

$$\alpha = \ln\left(\frac{d_N}{d_{N-1}}\right), \tag{3}$$

where d_{N-1} and d_N are the effective circular diameters of a site before and after the Nth shot, respectively, as measured by the robotic microscope. Furthermore, we will limit our analysis to damage sites with diameters in a narrow size range, between 50 and 100 μm, in the spirit of a single parameter study in which all other experimental parameters are held constant for data sets obtained with different pulse durations.

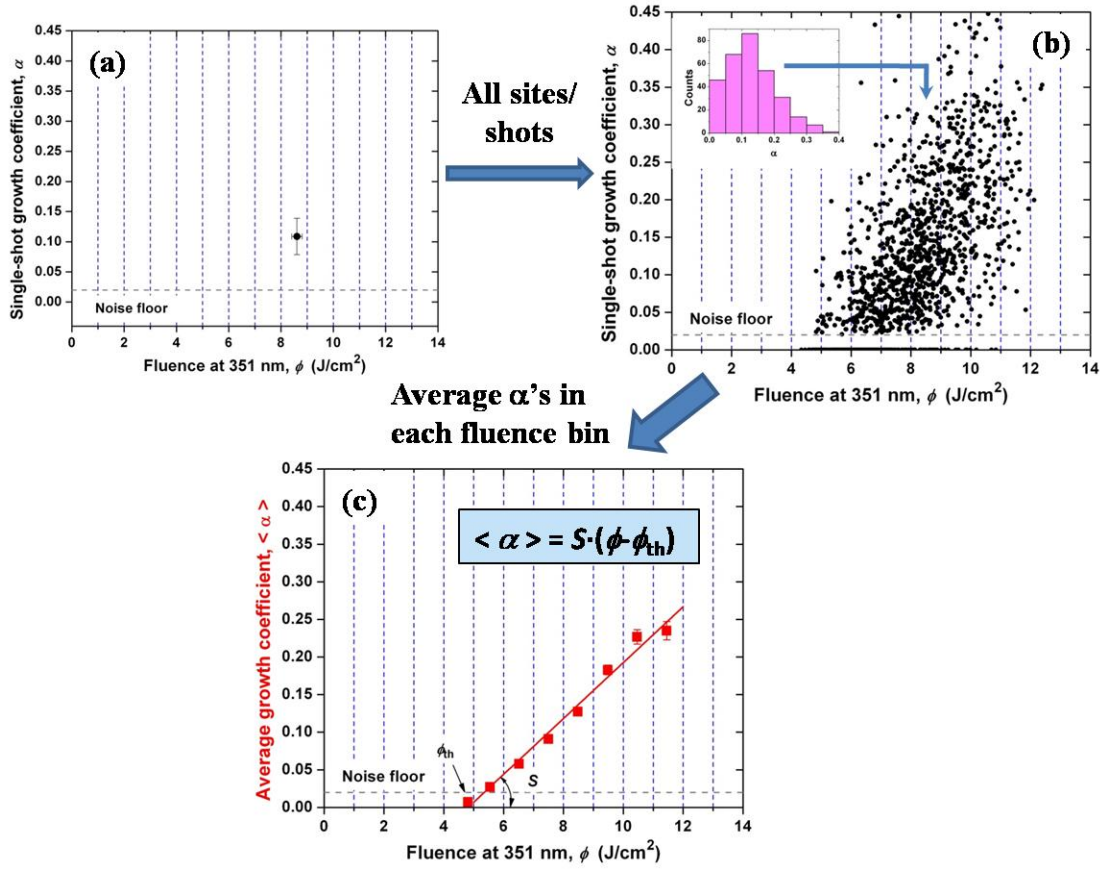

Figure 3 (color online). Three-step summary of data analysis based on the single-shot growth coefficient. (a) Each observed single shot growth coefficient α from Eq. (3) is plotted against the local fluence that produced it. (b) Plot α's for all shots and sites in a limited size range, i.e. 50-100 μm. Inset graph illustrates the distribution of α values in the 8-9 J/cm^2 fluence bin. (c) Average α values in 1 J/cm^2 fluence bins to reveal growth trends, i.e. average growth rate increases linearly with fluence.

The data analysis based on the single-shot growth coefficient proceeds as follows:

i) Each observed single shot growth coefficient, α, is plotted against the local fluence that produced it, as illustrated in Fig. 3(a). The fluence error bar in Fig. 3(a) represents the standard error of the mean fluence over a 1-mm patch centered at the site location. In addition, the error in the growth coefficient as calculated by Eq. (3) depends on size and is about 0.03 for an average site size of 75 μm. We also define the overall noise floor as the minimum perceived growth coefficient of ~0.02 due to sizing errors for the 50-100 μm size range, as shown by the dotted line in Figs. 3(a)-(c).

ii) We use Eq. (3) to compute α values for all sites/shots with sizes in the 50 to 100 μm range and plot them against the corresponding local fluence. By simultaneously growing ~50 sites, we quickly develop a large data set for a single pulse shape. This analysis step is illustrated in Fig. 3(b) for 5-ns FIT pulses, without the error bars on each data point for better clarity. We note the large spread in the data, which is well outside the measurement errors. By plotting the distribution of α values at fixed fluence, as shown in the inset graph of Fig. 3(b) for the fluence bin of 8-9 J/cm^2, we recognize the stochastic nature of the growth process leading to the observed spread in the data.

iii) We average the observed α values in 1 J/cm^2 fluence bins, as illustrated in Fig. 3(c). Here the error bars represent the uncertainty in the mean due to limited statistics, i.e. $se = \sqrt{\frac{s^2}{n}} = \sqrt{\frac{1}{n(n-1)}\sum_i (\alpha_i - \bar{\alpha})^2}$. The final step allows for

parameterization of the growth process, i.e. a linear dependence of the average growth coefficient on the mean fluence at 351 nm, as indicated by the line fit to the data in Fig. 3(c). The latter dependence is described as:

$$< \alpha >= S \cdot (\phi - \phi_{th}), \tag{4}$$

where the growth parameters are the rate of increase in growth coefficient with fluence, *S*, and the fluence threshold for growth, ϕ_{th}, respectively. It is important to note that the single-shot growth analysis reveals the same general growth trend as that derived by Norton et al. using a multi-shot approach. Specifically, Eqs. (2) and (4) have identical fluence functional dependencies, but the coefficients in Eq. (4) are expected to depend on pulse duration, size and other parameters.

4. RESULTS

In the following, we will be discussing the behavior of the mean $<\alpha>$ vs. fluence at different pulse durations. We have performed growth experiments with 1 ns, 2 ns, 5 ns, 10ns, and 15 ns FIT pulses with fluences ranging from 4 J/cm^2 to 12 J/cm^2. This fluence range is typically achieved in three separate growth experiments at the nominal fluences of 5, 8 and 11 J/cm^2. Specifically, the combination of 15% shot-to-shot variation in the average fluence and the spatial beam contrast provides ±1.5 J/cm^2 coverage around the target fluence.

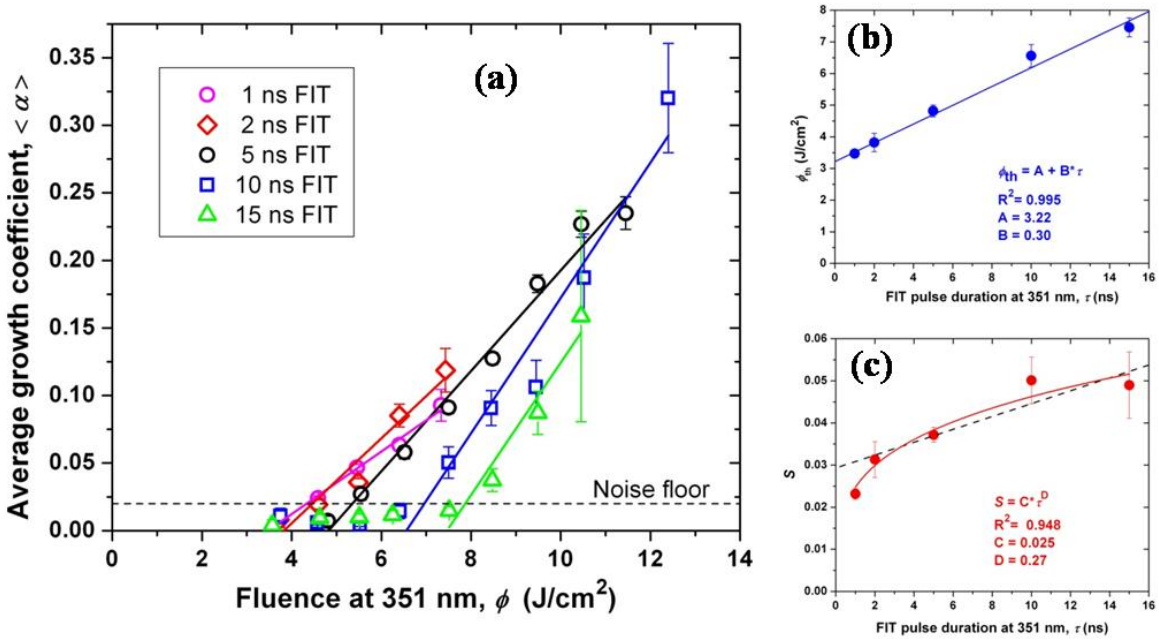

Figure 4 (color online). (a) The average growth coefficient vs. fluence at 351 nm for various FIT pulse durations of 1 ns to 15 ns. The linear fits to the data according to Eq. (4) are also shown by the solid lines. The growth threshold, ϕ_{th}, (b) and the rate of increase in growth coefficient with fluence, *S*, (c) exhibit a pulse duration dependence of $\sim \tau^{0.3}$.

By applying the single-shot analysis discussed in the previous section, we can reduce the data at different pulse durations to the average growth coefficient as a function of fluence, as shown in Fig. 4(a). Here the error bars represent the uncertainty in the mean due to limited statistics. We note that the single parameter study approach used in this work allows for a direct comparison between data sets in Fig. 4(a), where all the experimental parameters were held constant except for the pulse duration. The linear fits to the data according to Eq. (4) are also shown by the solid lines. These results demonstrate that the pulse duration has a significant impact on the growth of exit surface damage at 351 nm in the

1 ns to 15 ns range. Specifically, both the growth threshold and slope of $<\alpha>$ vs. ϕ increase with pulse duration, which is in contrast to previous beliefs based on limited data[2].

We extract the pulse duration dependence of the growth parameters using Eq. (4). Figure 4(b) shows the dependence of the growth threshold, ϕ_{th}, on pulse duration and Fig. 4(c) shows the dependence of the rate of increase in growth coefficient with fluence, *S*. To a first order, these parameters exhibit a nearly linear dependence on pulse duration from ~2 ns to 15 ns. However, for the case of shorter pulses of 1 ns and 2 ns, the growth parameters deviate from the general trend of linear dependence on pulse duration. The dependence of the growth parameters on pulse duration over the entire range is better described using a power law dependence with the coefficients shown in Fig. 4(b) and 4(c). Here the solid and dashed lines represent the power law vs. linear fits, respectively. Based on these results, we conclude that exit surface damage growth scales with pulse duration as $\sim\tau^{0.3}$ from 1 ns to 15 ns (FIT pulses) and for sites with diameters from 50 to 100 μm.

5. SUMMARY

We have presented a multi-site parallel damage growth technique using a large aperture laser with flexible pulse durations at 351 nm. Large data sets were reduced to the average growth coefficient vs. fluence vs. pulse duration based on the single-shot growth coefficient. This study demonstrates, for the first time, a significant dependence of exit damage growth parameters on pulse duration from 1 ns to 15 ns as $\tau^{0.3}$ for sites in the 50-100 μm size range. Future work will be aimed at elucidating the damage morphology and pulse shape dependence of growth at 351 nm for both input and exit surfaces of silica optics with the final goal of developing accurate predictive models and understanding the damage growth mechanisms at a fundamental level.

ACKNOWLEDGEMENTS

We thank W. A. Steele, J. J. Adams, M. Bolourchi and the OSL team for assistance in the sample preparation and execution of the experiments. This work was performed under the auspices of the U.S. Department of Energy by Lawrence Livermore National Laboratory under Contract DE-AC52-07NA27344.

REFERENCES

[1] Kozlowski, M. R., Mouser, R., Maricle, S., Wegner, P., and Weiland, T., "Laser damage performance of fused silica optical components measured on the Beamlet laser at 351 nm," Proc. SPIE 3578, 436-445 (1999).

[2] Norton, M. A., Hrubesh, L. W., Wu, Z., Donohue, E. E., Feit, M. D., Kozlowski, M. R., Milam, D., Neeb, K. P., Molander, W. A., Rubenchik, A. M., Sell, W. D., and Wegner, P., "Growth of laser initiated damage in fused silica at 351 nm," Proc. SPIE 4347, 468 (2001).

[3] Razè, G., Morchain, J. –M., Loiseau, M., Lamaignère, L., Josse, M., and Bercegol, H., "Parametric study of the growth of damage sites on the rear surface of fused silica windows," Proc. SPIE 4932, 127-135 (2003).

[4] Norton, M. A., Donohue, E. E., Hollingsworth, W. G., McElroy, J. N., and Hackel, R. P., "Growth of laser initiated damage in fused silica at 527 nm," Proc. SPIE 5273, 236-243 (2004).

[5] Norton, M. A., Donohue, E. E., Hollingsworth, Feit, M. D., Rubenchik, A. M., and Hackel, R. P., "Growth of laser initiated damage in fused silica at 1053 nm," Proc. SPIE 5647, 197-205 (2005).

[6] Norton, M. A., Donohue, E. E., Feit, M. D., Hackel, R. P., Hollingsworth, W. G., Rubenchik, A. M., and Spaeth, M. L., "Growth of laser damage in SiO2 under multiple wavelength irradiation," Proc. SPIE 5991, 599108 (2005).

[7] Lamaignère, L., Reyne, S., Loiseau, M., Poncetta, J. –C., and Bercegol, H., "Effects of wavelengths combination on initiation and growth of laser-induced surface damage in SiO_2," Proc. SPIE 6720, 67200F (2007).

[8] Norton, M. A., Carr, A. V., Carr, C. W., Donohue, E. E., Feit, M. D., Hollingsworth, W. G., Liao, Z., Negres, R. A., Rubenchik, A. M., and Wegner, P., "Laser damage growth in fused silica with simultaneous 351 nm and 1053 nm irradiation," Proc. SPIE 7132, 71321H (2008).

[9] Carr, C. W., Trenholme, J. B., and Spaeth, M. L., "Effect of temporal pulse shape on optical damage," Appl. Phys. Lett. 90 (4), 041110 (2007).

[10] Carr, C. W., Matthews, M. J., Bude, J. D., and Spaeth, M. L., "The effect of laser pulse duration on laser-induced damage in KDP and SiO_2," Proc. SPIE 6403, K4030 (2007).

[11] Carr, C. W., Cross, D., Feit, M. D., and Bude, J. D., "Using shaped pulses to probe energy deposition during laser-induced damage of SiO_2 surfaces," Proc. SPIE 7132, 71321C (2008).
[12] Norton, M. A., Donohue, E. E., Feit, M. D., Hackel, R. P., Hollingsworth, W. G., Rubenchik, A. M., and Spaeth, M. L., "Growth of laser damage on the input surface of SiO2 at 351 nm," Proc. SPIE 6403, 64030L (2007).
[13] Huang, W. Q., Han, W., Wang, F., Xiang, Y., Li, F. Q., Feng, B., Jing, F., Wei, X. F., Zheng, W. G., and Zhang, X. M., "Laser –induced damage growth on large aperture fused silica optical components at 351 nm," Chin. Phys. Lett. 26 (1), 017901 (2009).
[14] Norton, M. A., Adams, J. J., Carr, C. W., Donohue, E. E., Feit, M. D., Hackel, R. P., Hollingsworth, Jarboe, J. A., Matthews, M. J., Rubenchik, A. M., and Spaeth, M. L., "Growth of laser damage in fused silica: diameter to depth ratio," Proc. SPIE 6720, 67200H (2007).
[15] Bercegol, H., Lamaignère, L., Le Garrec, B., Loiseau, M., and Volto, P., "Self-focusing and rear surface damage in a fused silica window at 1064 nm and 355 nm," Proc. SPIE 4932, 276-285 (2003).
[16] Salleo, A., Chinsio, R., and Genin, F. Y., "Crack propagation in fused silica during UV and IR ns-laser illumination," Proc. SPIE 3578, 456-471 (1999).
[17] Courchinoux, R., Razè, G., Sudre, C., Josse, M., Boscheron, A., Lepage, C., Mazataud, E., Bordenave, E., Lamaignère, L., Loiseau, M., Donval, T., and Bercegol, H., "Laser-induced damage growth with small and large beams. Comparison between laboratory experiments and large-scale laser data," Proc. SPIE 5273, 99-106 (2004).
[18] Nostrand, M. C., Weiland, T. L., Luthi, R. L., Vickers, J. L., Sell, W. D., Stanley, J. A., Honig, J., Auerbach, J. Hackel, R. P., and Wegner, P., "A large aperture, high energy laser system for optics and optical components testing," Proc. SPIE 5273 325-333 (2004).
[19] Xu, S. Z., Lv, H. B., Yuan, X. D., Huang, J., Jiang, X. D., Wang, H. J., Zu, X. T., and Zheng, W. G., "Effects of vacuum on fused silica UV damage," Chin. Phys. Lett. 25 (1), 223-226 (2008).
[20] Xu, S. Z., Yuan, X. D., Yin, W., Xiang, X., and Zu, X. T., "Effect of UV laser conditioning on fused silica in vacuum," Opt. Mater. 31 (6) (2009).
[21] Carr, C. W., Feit, M. D., Nostrand, M. C. and Adams, J. J., "Techniques for qualitative and quantitative measurement of aspects of laser-induced damage important for laser beam propagation," Meas. Sci. Technol. 17 (7), 1958-1962 (2006).